biguously from fitting Equation 2 to the experimental data. The 2PA cross-section δ is determined by means of the expression

$$\delta = h\nu\beta/N \quad (4)$$

where N is the number of molecules per cm^3 and $h\nu$ is the excitation photon energy. Usually, δ is expressed in Göppert Mayer (GM) units, in which 1 GM $\equiv 1 \times 10^{-50}$ cm^4 s nm, using an optical parametric amplifier (TOPAS, from Light Conversion) pumped by 150 fs pulses at 775 nm, delivered by a commercial Ti:sapphire chirped pulse amplified system CPA-2001 from Clark-MXR Inc., operating at a 1 kHz repetition rate. The full width at half maximum (FWHM) pulse duration was 120 fs, and the spatial profile of the laser beam presented a Gaussian distribution. The beam waist size and pulse irradiance were determined via *Z*-scan measurements on fused silica (1.2 mm) [36]. The transmitted signal was monitored using a simple silicon positive instrinsic negative (PIN) photodetector coupled to a lock-in amplifier.

Two-photon-induced fluorescence measurements from 500 to 730 nm were carried out using the same laser system described above operating at 770 nm. The emission was dispersed by a monochromator and collected by a standard photomultiplier coupled to a lock-in amplifier. 2PA fluorescence emission intensity versus incident intensity was performed by changing the laser power with polarizers. Optical limiting measurements were carried out with the pump laser beam from the above-mentioned laser at 770 nm focused on a 2 mm thick quartz cuvette. The pump intensity was controlled with the same attenuator used in the fluorescence measurements. All measurements were performed at room temperature.

Received: March 14, 2005
Final version: April 14, 2005

[1] G. S. He, L. X. Yuan, Y. P. Cui, M. Li, P. N. Prasad, *J. Appl. Phys.* **1997**, *81*, 2529.
[2] A. Abbotto, L. Beverina, R. Bozio, A. Facchetti, C. Ferrante, G. A. Pagani, D. Pedron, R. Signorini, *Org. Lett.* **2002**, *4*, 1495.
[3] R. H. Kohler, J. Cao, W. R. Zipfel, W. W. Webb, M. R. Hanson, *Science* **1997**, *276*, 2039.
[4] W. Denk, J. H. Strickler, W. W. Webb, *Science* **1990**, *248*, 73.
[5] W. H. Zhou, S. M. Kuebler, K. L. Braun, T. Y. Yu, J. K. Cammack, C. K. Ober, J. W. Perry, S. R. Marder, *Science* **2002**, *296*, 1106.
[6] K. D. Belfield, K. J. Schafer, Y. U. Liu, J. Liu, X. B. Ren, E. W. Van Stryland, *J. Phys. Org. Chem.* **2000**, *13*, 837.
[7] K. D. Belfield, X. B. Ren, E. W. Van Stryland, D. J. Hagan, V. Dubikovsky, E. J. Miesak, *J. Am. Chem. Soc.* **2000**, *122*, 1217.
[8] J. D. Bhawalkar, G. S. He, P. N. Prasad, *Rep. Prog. Phys.* **1996**, *59*, 1041.
[9] K. D. Belfield, A. R. Morales, B. S. Kang, J. M. Hales, D. J. Hagan, E. W. Van Stryland, V. M. Chapela, J. Percino, *Chem. Mater.* **2004**, *16*, 4634.
[10] S. J. K. Pond, O. Tsutsumi, M. Rumi, O. Kwon, E. Zojer, J. L. Bredas, S. R. Marder, J. W. Perry, *J. Am. Chem. Soc.* **2004**, *126*, 9291.
[11] M. Albota, D. Beljone, J. L. Breda, J. E. Ehrlich, J. Y. Fu, A. A. Heikal, S. E. Hess, T. Kogej, M. D. Levin, S. Marder, D. McCord-Maughon, J. W. Perry, H. Rockel, M. Rumi, G. Subramanian, W. W. Webb, X. L. Wu, C. Xu, *Science* **1998**, *281*, 1653.
[12] K. D. Belfield, A. R. Morales, J. M. Hales, D. J. Hagan, E. W. Van Stryland, V. M. Chapela, J. Percino, *Chem. Mater.* **2004**, *16*, 2267.
[13] O. Mongin, L. Porres, L. Moreaux, J. Mertz, M. Blanchard-Desce, *Org. Lett.* **2002**, *4*, 719.
[14] J. Yoo, S. K. Yang, M. Y. Jeong, H. C. Ahn, S. J. Jeon, B. R. Cho, *Org. Lett.* **2003**, *5*, 645.
[15] G. P. Bartholomew, M. Rumi, S. J. K. Pond, J. W. Perry, S. Tretiak, G. C. Bazan, *J. Am. Chem. Soc.* **2004**, *126*, 11 529.
[16] G. Horowitz, F. Kouki, P. Spearman, D. Fichou, C. Nogues, X. Pan, F. Garnier, *Adv. Mater.* **1996**, *8*, 242.
[17] K. Ishii, K. Yakushi, H. Kuroda, H. Inokuchu, *Bull. Chem. Soc. Jpn.* **1984**, *57*, 3043.
[18] D. Schlettwein, A. Back, B. Schilling, T. Fritz, N. R. Armstrong, *Chem*. Mater. **1998**, *10*, 601.
[19] H. G. Lohmannsroben, H. Langhals, *Appl. Phys. B* **1989**, *48*, 449.
[20] H. Langhals, *Chem. Phys. Lett.* **1988**, *150*, 321.
[21] J. Ivri, Z. Burshtein, E. Miron, R. Reisfeld, M. Eyal, *IEEE J. Quantum Electron.* **1990**, *26*, 1516.
[22] D. Duff, A. M. Hor, A. R. Melnyk, D. Teney, in *SPIE Hard Copy and Printing Materials, Media and Process* (Ed: J. Gaynor), SPIE, Bellingham, WA **1990**, *1253*, p. 183.
[23] B. R. Cho, K. H. Son, S. H. Lee, Y. S. Song, Y. K. Lee, S. J. Jeon, J. H. Choi, H. Lee, M. H. Cho, *J. Am. Chem. Soc.* **2001**, *123*, 10 039.
[24] M. Drobizhev, A. Karotki, M. Kruk, N. Z. Mamardashvili, A. Rebane, *Chem. Phys. Lett.* **2002**, *361*, 504.
[25] G. S. He, T. C. Lin, P. N. Prasad, R. Kannan, R. A. Vaia, L. S. Tan, *J. Phys. Chem. B* **2002**, *106*, 11 081.
[26] H. Lei, Z. L. Huang, H. Z. Wang, X. J. Tang, L. Z. Wu, G. Y. Zhou, D. Wang, Y. B. Tian, *Chem. Phys. Lett.* **2002**, *352*, 240.
[27] M. Adachi, Y. Murata, S. Nakamura, *J. Phys. Chem.* **1995**, *99*, 14 240.
[28] P. A. Antunes, C. J. L. Constantino, R. Aroca, J. Duff, *Appl. Spectrosc.* **2001**, *55*, 1341.
[29] M. Sheik-Bahae, A. A. Said, E. W. Van Stryland, *Opt. Lett.* **1989**, *14*, 955.
[30] M. Sheik-Bahae, A. A. Said, T. H. Wei, D. J. Hagan, E. W. Van Stryland, *IEEE J. Quantum Electron.* **1990**, *26*, 760.
[31] L. De Boni, C. J. L. Constantino, L. Misoguti, R. F. Aroca, S. C. Zilio, C. R. Mendonca, *Chem. Phys. Lett.* **2003**, *371*, 744.
[32] I. N. Kang, D. H. Hwang, H. K. Shim, *Macromolecules* **1996**, *29*, 165.
[33] J. D. Bhawalkar, G. S. He, C. K. Park, C. F. Zhao, G. Ruland, P. N. Prasad, *Opt. Commun.* **1996**, *124*, 33.
[34] G. S. He, R. Helgeson, T.-C. Lin, Q. Zheng, F. Wudl, P. N. Prasad, *IEEE J. Quantum Electron.* **2003**, *39*, 1003.
[35] Q. Zheng, G. S. He, T.-C. Lin, P. N. Prasad, *J. Mater. Chem.* **2003**, *13*, 2499.
[36] D. Milan, *Appl. Opt.* **1998**, *38*, 546.

Novel Nanopyramid Arrays of Magnetite**

By *Fei Liu*, *Peijiang Cao*, *Huairuo Zhang*, *Jifa Tian*, *Congwen Xiao*, *Chengmin Shen*, *Jianqi Li*, and *Hongjun Gao**

Highly ordered magnetic metal nanowire arrays have been the focus of nanofabrication and nanotechnology for their potential applications in high-density storage and magneto-

[*] Prof. H. J. Gao, F. Liu, H. R. Zhang, J. F. Tian, C. W. Xiao, Dr. C. M. Shen, J. Q. Li
Beijing National Laboratory for Condensed Matter Physics
Institute of Physics
Chinese Academy of Sciences
Beijing 100080 (P.R. China)
E-mail: hjgao@aphy.iphy.ac.cn
Dr. P. J. Cao
Department of Material Science & Engineering
School of Science, Shenzhen University
Guangdong 518060 (P.R. China)

[**] This work is supported in part by the National 863 and 973 projects, and the National Science Foundation of China.

 DOI: 10.1002/adma.200500367

ADVANCED MATERIALS

optical devices.[1–6] Among magnetic metals, iron oxide is becoming more and more attractive because of its intrinsic half-metallic ferromagnetic nature, which can be widely used in catalysts,[7–9] biological assays,[10–13] chemical sensors,[14,15] and superparamagnets.[16] In the past years, much effort has been devoted to the preparation of nanoparticles, thin films, and bulk materials. But just a few approaches[17–21] have been developed to prepare one-dimensional magnetite nanowires, nanorods, and nanotubes. For example, Kumar et al.[17] prepared magnetite nanorods by ultrasound irradiation of iron acetate solutions. By using the supercritical fluid phase inclusion technique, Crowley et al.[18] grew magnetite nanotubes in mesoporous silica powder. Single-crystalline Fe_3O_4 nanowires were synthesized in an autoclave through hydrothermal processes.[19,20] Xue et al.[21] also fabricated polycrystalline magnetite nanowires in an anodic aluminum oxide (AAO) template by electrodeposition. However, highly ordered single-crystalline magnetite arrays were not reported until now.

Here, we present the fabrication of large-scale, single-crystalline Fe_3O_4 nanopyramid arrays by CH_4 and N_2 plasma sputtering of hematite (0001) wafers *without using any template or catalyst*. The morphology, structure, and magnetic properties of magnetite nanopyramids were characterized by scanning electron microscopy (SEM), transmission electron microscopy (TEM), and vibrating sample magnetometry (VSM). The possible growth mechanism is also discussed.

SEM images of magnetite samples synthesized on a hematite [0001] substrate at different growth times are shown in Figure 1. Large-area Fe_3O_4 nanopyramid arrays were obtained by controlling the experimental conditions. As shown in Figure 1A, after a two-hour sputtering time, large-area, aligned magnetite nanopyramids stand vertically on the hematite substrate. The side view of the Fe_3O_4 nanostructure is shown in Figure 1B, in which one can see that the structures have a uniform, pyramid-like shape with a length of about 3 μm. It can also be found that the diameter of the Fe_3O_4 pyramid gradually decreases from 500 nm (the cap) to 100 nm (the bottom) vertically. The profile of the nanostructure looks like an "Egyptian pyramid" with many layers. To investigate the detailed morphology, the top view of the nanopyramids is given in Figure 1C, and a high-resolution SEM image of the top part of a typical Fe_3O_4 nanopyramid is shown in Figure 1D. It can be seen that the cap of the nanopyramid is a perfect pyramid consisting of four triangular faces and one rectangular base. The mean size of the cap is about 400–500 nm. For analyzing the influence of growth time on the sample morphology, we prepared a series of samples at different reaction times. Figure 1E is an SEM image of the sample sputtered in the plasma for five minutes. One can see that the bulk Fe_3O_4 structure with a pyramid shape was formed on the Fe_2O_3 substrate. Figure 1F is a typical SEM image of the sample sputtered for 20 min, indicating that more and more nanometer-sized Fe_3O_4 pyramids came into being during the reaction. In the inset in Figure 1F, the initial stage of Fe_3O_4 nanopyramid growth is clearly observed on top of the bulk pyramid. From the images of Figure 1, we can conclude the sputtering of the plasma on the α-Fe_2O_3 substrate might be beneficial for the formation of the magnetite nanopyramids.

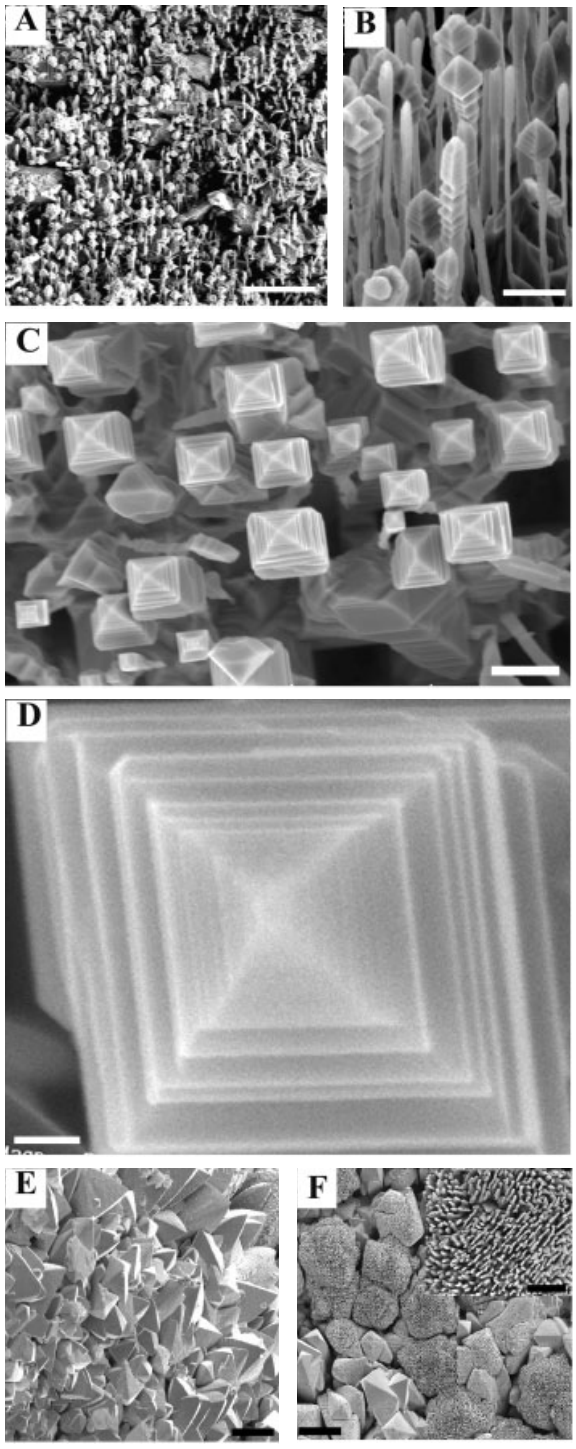

Figure 1. SEM images of Fe_3O_4 structures at different growth times. A) Low-magnification image of large-area Fe_3O_4 nanopyramid arrays (2 h). Scale bar: 5 μm. B) Side view and C) top view of the nanopyramids. Scale bars: 1 μm (B) and 0.5 μm (C). D) High-resolution image of the nanopyramid cap. Scale bar: 100 nm. E,F) SEM images of the samples at growth times of 5 and 20 min. Scale bars: 10 μm. Inset in (F): high-magnification image of the sample (20 min). Scale bar: 2 μm.

In order to determine the detailed crystalline structure, TEM and high-resolution TEM (HRTEM) measurements were employed to investigate the sample. A typical TEM image of a Fe_3O_4 nanopyramid is shown in Figure 2A. The diameter of the nanopyramid gradually decreases from the top to the bottom, which is in good agreement with the image shown in Figure 1B. Figure 2B provides the corresponding selected-area electron diffraction (SAED) pattern. Our energy-dispersive X-ray absorption spectroscopy results show that this novel structure is composed of Fe and O. From the SAED pattern, the crystal structure of this novel nanomaterial is identified to be the Fe_3O_4 phase, which is consistent with the data of the Joint Committee for Powder Diffraction Standards (JCPDS) card No. 19-629. Moreover, the pattern indicates that the magnetite nanopyramids grow along [001] and the nanopyramids are perfect single crystals. By analyzing the HRTEM image (Fig. 2C), we prove that the Fe_3O_4 nanopyramid has an inverse spinel structure and the spacing, *d*, between adjacent (001) growth planes is 2.095 Å. To clarify the chemical composition of the nanopyramid, the electron energy-loss spectroscopy (EELS) analysis is shown in Figure 3. It reveals that the characteristic oxygen K-shell ionization edge (~532 eV, 542 eV) and the ionization edge (~712 eV, ~726 eV) corresponding to the Fe L_2 and Fe L_3 shells, respectively. The Gatan EELS Analysis software provided with the TEM (Tecnai F20) is used to quantitatively analyze the EELS spectra of several nanopyramids. It demonstrates that the average atomic ratio of the Fe to O elements is 3:4, which further confirms the as-prepared nanopyramid to be the Fe_3O_4 phase.

A measurement of the magnetic properties of the sample at room temperature is presented in Figure 4. It can be clearly seen that the nanopyramid has a saturation magnetization of 52.5 emu g^{-1} and a coercive field of 79.0 Oe, which is lower than the values of bulk Fe_3O_4. The saturation magnetization and the coercive field of bulk Fe_3O_4 are about 85–100 emu g^{-1} and 115–150 Oe, respectively. The deviation is likely due to the sample nanostructure because the magnetization of samples consisting of small particles decreases with decreasing particle size. The increase of the dispersion in the exchange integral reaches a superparamagnetic state wherein each particle acts as a big spin with a suppressed exchange interaction between the particles.[22]

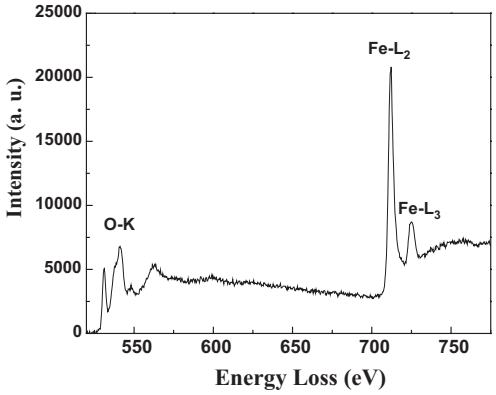

Figure 3. EELS spectrum of the Fe_3O_4 nanopyramid, indicating the oxygen K-shell ionization edge (~532 eV, 542 eV) and the Fe L_2 and Fe L_3 shell ionization edges (~712 eV, ~726 eV).

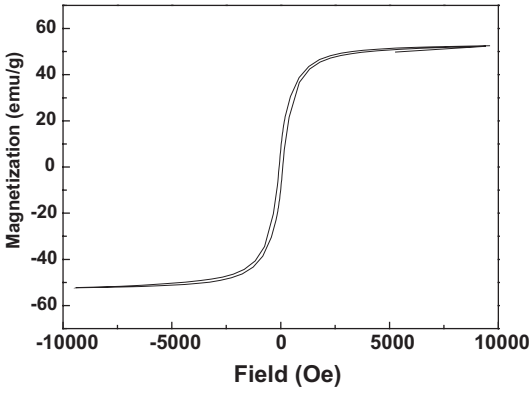

Figure 4. The room-temperature magnetic hysteresis curve of the nanopyramid. It has a saturation magnetization of 52.5 emu g^{-1} and a coercive field of 79.0 Oe. (1 emu = 10^{-3} A m^2, 1 Oe = $10^3/4\pi$ A m^{-1}.)

The morphology of Fe_3O_4 nanopyramids is distinctly different from the nanowires and nanorods. Moreover, catalysts, a mixture of metal and metal oxide, or reaction gases including iron element were not used during the reaction process. Therefore, the vapor–liquid–solid (VLS), vapor–solid (VS), or oxide-assisted growth (OAG) mechanisms cannot be used to explain the growth of the nanopyramid. We speculate that the nanopyramid growth mainly resulted from the plasma sputtering of the Fe_2O_3(0001) substrate during the reaction process.

Why does the magnetite pyramid form on the surface of the α-Fe_2O_3 substrate? To understand the growth mechanism, a schematic diagram of the possible growth process is shown in Figure 5. 1) The mixed gas of N_2 and CH_4 forms the plasma under microwave irradiation and reconstruction from α-Fe_2O_3(0001) to Fe_3O_4(111) tends to take place on

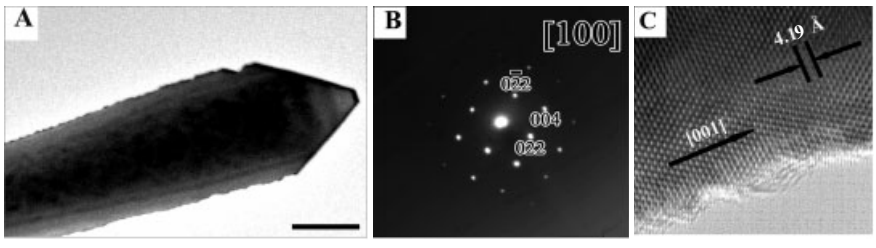

Figure 2. TEM and HRTEM images taken from the magnetite nanopyramid. A) Typical TEM image of the nanopyramid. Scale bar: 100 nm. B) The corresponding SAED pattern. C) HRTEM image of the same sample. Scale bar: 10 Å.

ADVANCED MATERIALS

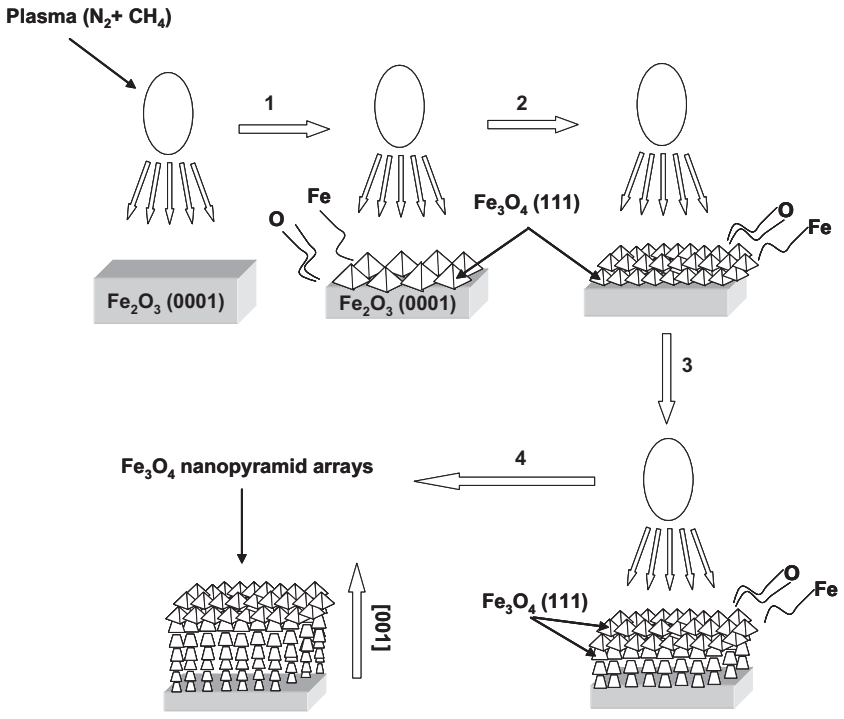

Figure 5. Schematic illustration of the growth process for magnetite nanopyramids. Bulk pyramid-like structures form in Step 1. In Step 2, more nanopyramids with nanometer size come into being. In Step 3, nanopyramids begin to grow along the [001] orientation. Large-area nanopyramid arrays are prepared in Step 4.

the substrate under reductive conditions. Pyramid-like bulk Fe_3O_4 structures are fabricated, then reconstruction on the α-Fe_2O_3(0001) surface takes place. Figure 1E provides evidence of this stage. 2) The surface covered by many big Fe_3O_4 pyramids changes into a surface consisting of many nanometer-sized magnetite nanopyramids during the bombardment of the mixed gas plasma, which is consistent with the SEM image shown in Figure 1F. 3) The base plane of Fe_3O_4 nanopyramid grows epitaxially on the α-Fe_2O_3(0001), and the initial growth stage of nanopyramid arrays occurs when the reaction proceeds. The existence of this stage is also proven by the SAED pattern. 4) High-density magnetite nanopyramid arrays are prepared in the orientation perpendicular to the hematite substrate.

We propose the following to explain the formation of Fe_3O_4(111) under reductive conditions. First, the close-packed oxygen layer lying parallel to the Fe_3O_4(111) (surface constant: 5.03 Å) is similar to α-Fe_2O_3(0001) (surface constant: 5.92 Å) crystallographically.[23,24] Second, the plasma bombardment removes more oxygen atoms from the surface region than iron atoms, thereby creating a disordered and reduced selvedge where Fe_3O_4 reconstruction takes place.[24,25] On the oxygen-deficient surface, partial octahedral iron sites in α-Fe_2O_3 are possibly replaced by ordered tetrahedral iron sites,[25] inducing the transition in the appearance of Fe_3O_4. Last, the Fe_3O_4{111} plane is the most energetically stable crystalline plane in nature. Possible reasons for the appearance of multilayered structures are as follows: The plasma sputtering possibly takes fewer atoms from the {111} plane than it does from other planes and makes the side planes tend to be {111}, because the most stable plane for magnetite is {111}. In addition, the sputtering velocity is so rapid that the growth fronts do not have enough time to complete the growth of perfect pyramid-like structures. In this way, multilayered, pyramid-like structures growing along [001] form. In our work, the alignment of nanopyramids might be attributed to steric overcrowding[26,27] or a mutual repulsion force existing among these magnetic nanopyramids.

Plasma sputtering of hematite (0001) substrates provides a simple approach to the fabrication of large-area Fe_3O_4 nanopyramid arrays. The as-prepared nanopyramids perpendicular to the substrate are single crystals growing along the [001] direction. They are perfect Fe_3O_4 crystals with inverse spinel structure and their mean length is about 3 μm. Based on our results, the possible growth mechanism of magnetite nanopyramid arrays is discussed. This novel Fe_3O_4 nanostructure may have potential applications in constructing nanoscale magnetic devices and high-density storage media.

Experimental

A 2450 MHz microwave plasma chemical vapor deposition (MPCVD) system developed in our laboratory [28] was used to prepare the Fe_3O_4 nanopyramid arrays. The α-Fe_2O_3 [0001] wafer was used as the substrate. After being washed 10 min with acetone, alcohol, and deionized water in an ultrasonic cleaner, the hematite substrate was placed vertically on a quartz holder in the vacuum chamber. When the base pressure in the system was lower than 0.1 Pa, the mixed gas consisting of CH_4 and N_2 was introduced into the vacuum chamber at a flow rate ratio of 1:100 sccm (standard cubic centimeters per minute). The power of the microwave plasma was retained at 850 W and the deposition pressure of the mixed gas was kept at about 2600 Pa. After 2–3 h reaction time at a temperature of 800 °C, a dark film formed on the surface of the hematite substrate.

A field-emission type scanning electron microscope (XL-SFEG, FEI Corp.) was used to observe the morphologies of the Fe_3O_4 nanostructures. Transmission electron microscopy (Tecnai-20, FEI Corp.) and high-resolution transmission electron microscopy (Tecnai F20, FEI Corp.) were employed to investigate the Fe_3O_4 nanostructures. The room-temperature magnetic curve of the sample was obtained in a Lakeshore 7400 Series VSM System. Before the measurements of the magnetic properties were carried out, the sample was scratched from the substrate because hematite is also magnetic.

Received: February 21, 2005
Final version: April 25, 2005

[1] K. Dagani, *Science* **1991**, *254*, 1300.
[2] L. Gunther, *Phys. World* **1990**, *2*, 28.
[3] D. T. Gryko. F. Zhao, A. A. Yasseri, K. M. Roth, D. F. Bocian, W. G. Kuhr, J. S. Lindsey, *J. Org. Chem.* **2000**, *65*, 7356.
[4] S. Manalis, K. Babcock, J. Massie, V. Elings, K. Dugas, *Appl. Phys. Lett.* **1995**, *76*, 2585.
[5] S. Y. Chou, M. S. Wei, P. R. Krauss, P. B. Fisher, *J. Appl. Phys.* **1994**, *76*, 6673.
[6] K. Yamaguchi, K. Matsumoto, T. Fujii, *J. Appl. Phys.* **1990**, *67*, 233.
[7] M. A. Keane, *J. Catal.* **1997**, *166*, 347.
[8] J. W. Geus, *Appl. Catal.* **1986**, *25*, 313.
[9] H. H. Kung, *Transition Metal Oxides: Surface Chemistry and Catalysis*, Elsevier, New York **1989**.
[10] M. DeCuyper, M. Joniau, *Prog. Colloid Polym. Sci.* **1990**, *82*, 353.
[11] T. Yoshimoto, T. Mihama, K. Takahashi, Y. Saito, Y. Saito, Y. Tamura, Y. Inda, *Biochem. Biophys. Res. Commun.* **1987**, *145*, 908.
[12] K. Raj, R. Moskowitz, *J. Magn. Magn. Mater.* **1990**, *85*, 233.
[13] B. R. Martin, D. J. Dermody, B. D. Reiss, M. M. Fang, L. A. Lyon, M. J. Natan, T. E. Mallouk, *Adv. Mater.* **1999**, *11*, 1021.
[14] L. Huo, W. Li, L. Lu, H. Cui, S. Xi, J. Wang, B. Zhao, Y. Shen, Z. Lu, *Chem. Mater.* **2000**, *12*, 790.
[15] J. Handley, *Anal. Chem.* **2002**, *74*, 196.
[16] J. Kvassilion, V. Mehrotra, M. W. Russel. E. P. Giannelis, R. D. Shull, R. F. Ziolo, *J. Appl. Phys.* **1993**, *73*, 5109.
[17] R. V. Kumar, Y. Koltypin, X. N. Xu, Y. Yeshurun, A. Gedanken, I. Felner, *J. Appl. Phys.* **2001**, *89*, 6324.
[18] T. A. Crowley, K. J. Ziegler, D. M. Lyons, D. Erts, H. Olin, M. A. Morris, J. D. Holmes, *Chem. Mater.* **2003**, *15*, 3518.
[19] J. Wang, Q. W. Chen, C. Zeng, B. Y. Hou, *Adv. Mater.* **2004**, *16*, 137.
[20] L. Q. Xu, W. Q. Zhang, Y. W. Ding, Y. Y. Peng, S. Y. Zhang, W. C. Yu, Y. T. Qian, *J. Phys. Chem. B* **2004**, *108*, 10 859.
[21] D. S. Xue, L. Y. Zhang, C. X. Gao, X. F. Xu, A. B. Gui, *Chin. Phys. Lett.* **2004**, *21*, 733.
[22] S. R. Elliott, *Physics of Amorphous Materials*, Longman, London **1984**, p. 350.
[23] N. G. Condon, F. M. Leibsle, A. R, Lennie, P. W. Murray, T. M. Parker, D. J. Vaughan, G. Thornton, *Surf. Sci.* **1998**, *397*, 278.
[24] N. G. Condon, F. M. Leibsle, T. Parker, A. R. Lennie, D. J. Vaughan, G. Thornton, *Phys. Rev. B: Condens. Matter Mater. Phys.* **1997**, *55*, 15 885.
[25] R. A. Fellows, A. R. Lennie, H. Raza, C. L. Pang, G. Thornton, D. J. Vaughan, *Surf. Sci.* **2000**, *445*, 11.
[26] F. Liu, P. J. Cao, H. R. Zhang, H. J. Gao, C. M Shen, Z. Wang, J. Q. Li, *J. Cryst. Growth*, **2005**, *274*, 126.
[27] P. J. Cao, Y. S. Gu, H. W. Liu, F. Shen, Y. G. Wang, Q. F. Zhang, J. L. Wu, H. J. Gao, *J. Mater. Res.* **2003**, *18*, 1686.
[28] Y. S. Gu, Y. P. Zhang, Z. J. Duan, X. R. Chang, Z. Z. Tian, N. X. Chen, C. Dong, D. X. Shi, X. F. Zhang, L. Yuan, *J. Mater. Sci.* **1999**, *34*, 3117.

Microstructure and Electromechanical Properties of Carbon Nanotube/Poly(vinylidene fluoride—trifluoroethylene—chlorofluoroethylene) Composites**

By *Shihai Zhang*,* *Nanyan Zhang*, *Cheng Huang*, *Kailiang Ren*, and *Qiming Zhang*

Their nanometer-scale dimensions, along with their large shape anisotropy, high mechanical strength, and very high thermal and electrical conductivity, make carbon nanotubes (CNTs) an excellent material choice for nanocomposites, in which even a very small amount of CNTs can induce significant changes in the material's properties.[1–3] Whereas most of the reported studies were focused on the enhancement of mechanical properties and/or electrical conductivity of composites, in this communication we investigate the influence of CNTs on the microstructure and electromechanical properties of the electrostrictive terpolymer poly(vinylidene fluoride—trifluoroethylene—chlorofluoroethylene), abbreviated P(VDF-TrFE-CFE). It will be shown that the crystallinity, Young's modulus, dielectric constant, electrostrictive strain, and elastic energy density of P(VDF-TrFE-CFE) can be simultaneously improved by inclusion of only 0.5 wt.-% CNTs.

PVDF-based ferroelectric polymers are well known for their strong piezoelectricity. They can perform efficient electrical-to-mechanical energy conversion and generate large mechanical actuation in response to external electrical stimulation. Therefore, these polymers are attractive for a broad range of applications, such as sensors, actuators, artificial muscles, ferroelectric memory devices, and integrated microelectromechanical systems.[4,5] Recently, by employing defect modifications, such as by introducing a bulky third monomer CFE, it has been shown that the normal ferroelectric P(VDF-TrFE) can be converted into a ferroelectric relaxor P(VDF-TrFE-CFE), and the electromechanical response can be significantly enhanced.[6,7] For instance, a hysteresis-free

[*] Dr. S. Zhang, Dr. N. Zhang, Dr. C. Huang, Prof. Q. M. Zhang
Materials Research Institute
The Pennsylvania State University
University Park, PA 16802 (USA)
E-mail: sqz100@psu.edu
K. Ren, Prof. Q. M. Zhang
Department of Electrical Engineering
The Pennsylvania State University
University Park, PA 16802 (USA)
Prof. Q. M. Zhang
Department of Materials Science and Engineering
The Pennsylvania State University
University Park, PA 16802 (USA)

[**] This project was supported by U.S. NIH under grant 8R01EB002078-04. We thank Dr. F. Bauer at ISL of France for the synthesis of the P(VDF-TrFE-CFE) terpolymer.

 DOI: 10.1002/adma.200500313